Deceleration and trapping of a fast supersonic beam of metastable helium atoms with a 44-electrode chip decelerator

P. Allmendinger, J. A. Agner, H. Schmutz, and F. Merkt

Laboratorium für Physikalische Chemie, ETH Zürich, CH-8093, Switzerland

A surface-electrode decelerator consisting of 44 electrodes has been used to decelerate supersonic beams of helium Rydberg atoms moving with an initial velocity of 1200 m/s. Prior to the deceleration, the helium atoms were excited from the $1s2s \, {}^1S_0$ metastable state to selected Rydberg-Stark states with a narrow-band tunable UV laser. Complete deceleration could be achieved over a distance of 36 mm and in 60 μs, corresponding to an acceleration of -2.0×10^7 m/s^2. After deceleration, the atoms were held in stationary electric traps above the chip surface, reaccelerated off the chip, and detected by pulsed electric-field ionization. The decelerator was also used to generate helium Rydberg-atom beams with a final velocity tunable between 0 and 1200 m/s. Transitions between low- and high-field-seeking Rydberg-Stark states were observed during trap loading and are attributed to adiabatic Landau-Zener dynamics at electric fields exceeding the Inglis-Teller field. By comparing the experimental results with the results of particle-trajectory simulations, the velocity distribution of the decelerated atoms was found to be characterized by temperatures ranging between 50 and 200 mK, depending on the magnitude of the electric dipole moment of the Rydberg-Stark states selected prior to the deceleration.

I. INTRODUCTION

Much progress has been made in the past 15 years in the development of experimental methods to manipulate the velocity of atoms and molecules in supersonic beams [1–4]. In particular, multistage Stark and Zeeman deceleration experiments were introduced to generate slow beams of translationally cold atoms and molecules and load them into electric and magnetic traps at temperatures in the range from 1 mK to 1 K. These samples have found applications in high-resolution spectroscopy [5], in the studies of inelastic and reactive collisions at low temperatures [6], in measurements of excited-state lifetimes [7,8] and as a first step to reach even lower temperatures with further cooling methods [9].

The methods and the types of instruments available for such experiments have been described in detail in several recent review articles [2–4] and include multistage Stark deceleration, multistage Zeeman deceleration, deceleration by optical [10] and microwave fields [11], Rydberg-Stark deceleration [12,13], and deceleration using moving-trap devices [14–16]. To reduce the size and complexity of the experiments and at the same time achieve larger decelerations, chip-based decelerator concepts have been realized recently [17,18], which open the prospect of manipulating molecules at the solid-gas interface, with potential applications in surface science [19,20], quantum-information science [21], and laboratory-on-a-chip-type applications [22].

In this article, we present the results of experiments in which we have used a Rydberg-Stark surface-electrode decelerator to slow down a fast beam of He and trap the atoms at a density of 4×10^5 cm^{-3} above the decelerator surface. This surface decelerator is an extension of a proof-of-principle device used to decelerate and trap Rydberg hydrogen atoms. Being able to decelerate and trap helium Rydberg atoms close to chip surfaces may, in the future, enable one to overcome some of the difficulties encountered in quantum-optics experiments in which alkali-metal Rydberg atoms have been used near chip surfaces [23–26]: The problems associated with the deposition

of alkali-metal atoms onto the surface, such as the creation of patches and inhomogeneous electric fields, can be avoided with He. We also show that the characteristics of our decelerator make it suitable to decelerate a wide range of atoms and molecules.

II. EXPERIMENT

The experimental setup is presented schematically in Fig. 1 and consists of (i) a source chamber where a pulsed supersonic beam of metastable helium atoms in the $1s2s \, {}^1S_0$ state (referred to as metastable He hereafter) is generated, (ii) a photoexcitation region where these atoms are photoexcited to selected Rydberg-Stark states with principal quantum number n in the range between 25 and 35, (iii) the actual surface-electrode decelerator, and (iv) a detection region where the decelerated Rydberg atoms are field ionized and the He$^+$ ions are extracted toward a microchannel-plate detector by applying a pulsed voltage across a stack of five resistively coupled extraction plates. The decelerator is an extended version of the proof-of-principle 11-electrode decelerator we recently developed to decelerate hydrogen atom beams [17]. Of particular relevance for the results presented in this article are the following improvements compared to the earlier design described in Ref. [17]: The photoexcitation is now carried out between two metallic plates with surfaces parallel, rather than perpendicular, to the atomic-beam propagation axis, which enables the preparation of Rydberg-Stark states in a more homogeneous electric field. The bandwidth of the laser used to prepare the Rydberg-Stark state was reduced to 200 MHz, which makes it possible to fully resolve all Stark states at n values below 40. The distance between the Rydberg-atom beam and the surface can now be adjusted by displacing the position where the UV laser beam crosses the atomic beam to optimize the number of atoms loaded into the moving traps of the decelerator. For the experiments presented in this article, a distance of 0.75 mm was chosen and a slit was mounted at
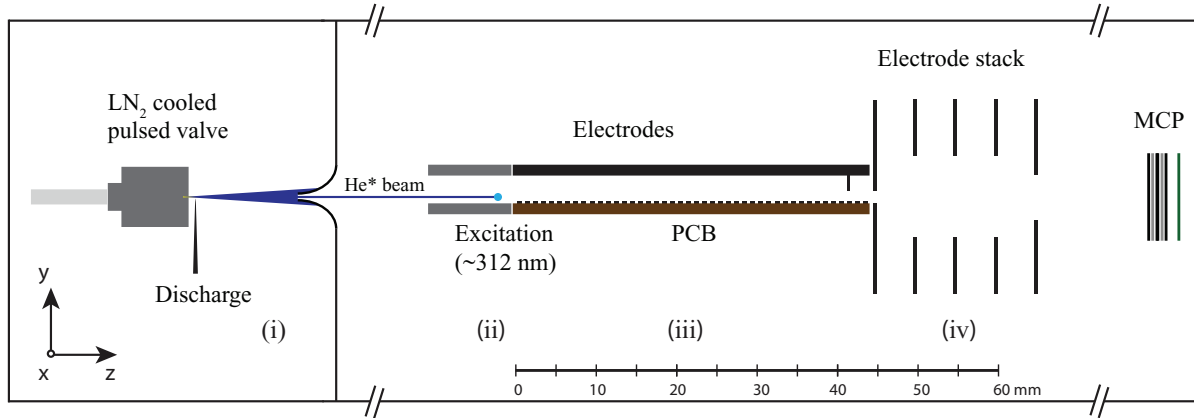
FIG. 1. (Color online) Schematic diagram of the 44-electrode Rydberg-Stark decelerator used to decelerate beams of helium atoms moving initially at a velocity of 1200 m/s: (i) source chamber, (ii) photoexcitation region, (iii) surface-electrode decelerator, and (iv) detection region.

the end of the decelerator that restricts the detection to atoms located within 1 mm from the decelerator surface. The length of the decelerator was extended from 11 mm (11 electrodes) to 44 mm (44 electrodes), which makes it suitable to decelerate beams of a wider range of atoms and molecules. Finally, the detection region at the end of the decelerator now consists of a 2-cm-long stack of five resistively coupled electrodes designed for the application of homogeneous fields and has been placed immediately after the decelerator (see Fig. 1).

FIG. 2. Spectrum of the $n = 30$ Rydberg-Stark states of He recorded following single-photon excitation from the metastable $1s2s\ ^1S_0$ state in the presence of an electric field of 35.7 V/cm. The Stark states are labeled with the value of k that represents the difference between the parabolic quantum numbers n_1 and n_2. The upper (lower) spectrum was obtained using UV laser radiation with the electric-field vector predominantly parallel (perpendicular) to the dc electric-field vector, resulting in the preferential production of $m_\ell = 0$ ($m_\ell = \pm 1$) Rydberg states. Weak transitions to $m_\ell = \pm 1$ ($m_\ell = 0$) Rydberg-Stark states are nevertheless observed. See the text for details.

The supersonic beam of metastable helium atoms was prepared by striking a pulsed electric discharge near the orifice of a pulsed valve operated at a repetition rate of 25 Hz and emitting 200-μs-long pulses of pure He, as described in Refs. [21,27,28]. To achieve an initial beam velocity of ≈ 1200 m/s, the body of the valve was connected thermally to a liquid-nitrogen reservoir. After collimation with a skimmer (Beam Dynamics, 1-mm-diam orifice) the supersonic beam was intersected at right angles by a UV laser beam employed to excite the atoms to Rydberg-Stark states. The photoexcitation was carried out between two parallel metallic plates used to apply a dc electric field in the photoexcitation region that was sufficiently homogeneous to enable the preparation of selected Stark states. The narrow-band UV radiation ($\lambda \approx 312$ nm) was generated from the cw output of a single-mode ring-dye laser operated at 624 nm with the dye kiton red after pulsed amplification in three dye cells pumped by the doubled output of a pulsed Nd:YAG laser and subsequent frequency doubling with a β barium borate crystal. The polarization of the UV laser could be adjusted with a half-wave plate to be parallel or perpendicular to the dc electric-field vector (see Fig. 1) so that photoexcitation predominantly resulted in the production of $m_\ell = 0$ and ± 1 Stark states, respectively. The excitation spectra to $m_\ell = 0$ (upper panel) and $m_\ell = \pm 1$ (lower panel) Rydberg-Stark states of principal quantum number $n = 30$ depicted in Fig. 2 were recorded at an electric field strength of 35.7 V/cm and illustrate the ability to fully resolve the different Stark states. The slight inhomogeneity of the electric field in the photoexcitation volume is revealed by the increasing inhomogeneous broadening with increasing value of $|k|$. The observation of weak transitions to $m_\ell = \pm 1$ Stark states in the upper spectrum and to $m_\ell = 0$ Stark states in the lower spectrum indicates that the polarization vector was not precisely parallel, or precisely perpendicular in the case of the lower panel, to the dc electric-field vector. Because all transitions are resolved and $m_\ell = 0$ and ± 1 states can be selected individually by choosing the appropriate frequencies, no effort was invested to adjust the polarization vectors more precisely.

At a distance of 2.5 mm beyond the excitation spot, the helium Rydberg-atom beam enters the actual decelerator, which consists of a printed circuit board (PCB) equipped with

44 parallel surface electrodes of 500 μm width and center-to-center spacing $d_z = 1$ mm along the beam propagation direction (z direction). Electric traps moving above the PCB in the direction of propagation of the supersonic beam were produced by applying oscillating voltages (called waveforms hereafter) of the form $V_i = (-1)^i V_0[1 + \cos(\omega t + \phi_i)]$ [i is an index running from 1 to 44 used to label the electrodes, $2V_0$ is the peak-to-peak amplitude, ω is the oscillation frequency, and $\phi_i = (2 - i)2\pi/3$ [17,29]] to the successive electrodes from opposite sides via point contacts in their enlarged base [see Fig. 2(a) of Ref. [17]]. These waveforms result in the formation of tubular traps of ≈ 4 mm length and a diameter of 0.5 mm, separated by 3 mm, and moving at a speed

$$v_z = 3d_z\omega/(2\pi) \tag{1}$$

in the beam propagation direction. As explained in Ref. [17], the electrode design leads to a phase-space acceptance that can be adjusted to the phase-space characteristics of the Rydberg-atom beam and enables the efficient loading of the Rydberg atoms into a single moving electric trap. In most experiments presented in this article, voltages V_0 of 40 V were applied, resulting in a trap depth of 54 V/cm, or ≈ 4 K for $n = 30$, $k = 29$, and $m_\ell = 0$ Rydberg states. The waveform switch-on time relative to the photoexcitation laser pulse can be adjusted so that all atoms with the selected velocity are loaded into a *single* trap, as illustrated in Fig. 3. This figure displays the Rydberg-atom signal detected by pulsed-field ionization at the end of the decelerator as a function of the switch-on time; the waveform frequency is selected to guide atoms above the decelerator surface at a constant velocity of 1210 m/s. At the earliest switch-on times, no signal is detected because the Rydberg atoms have not reached the decelerator yet when the waveforms are applied. At switch-on times beyond 2 μs, a regular oscillation is observed. The first maximum in the trace depicted in Fig. 3 corresponds to an experiment in which the excited Rydberg atoms were loaded into the trap located just upstream of the first electrode at the

waveform switch-on time, the second maximum to loading the Rydberg atoms in the trap located between the third and fourth electrodes, the third maximum to loading the atoms in the trap located between the sixth and seventh electrodes, etc. After five maxima (corresponding to atoms loaded between the 12th and 13th electrodes), the background signal between two maxima starts rising, because the atoms located outside the traps are not fully rejected by the waveforms over the distance separating them from the end of the decelerator.

Acceleration or deceleration is achieved by temporal variation of the oscillation frequency. In the experiments presented here, a linear frequency chirp $\omega(t) = (2\pi/3d_z)(v_z + a_z t)$ was applied to the waveforms, v_z corresponding to the initial velocity of the atoms and a_z to the desired acceleration. With suitably designed waveforms, the Rydberg atoms could be decelerated to zero velocity, stored for a predefined time interval, and accelerated again.

After the atoms leave the decelerator, they enter the detection region where they are ionized by a pulsed electric field of 2000 V/cm, which also extracts the ions toward a multichannel-plate detector. The synchronization of the valve opening time, the electric discharge used to produce the metastable atoms, the Nd:YAG laser used to pump the dye amplification stages, the waveform switch-on times, and the pulsed electric voltages used to field ionize the atoms at the end of the decelerator was achieved using a digital delay generator.

To determine the velocity distribution of the Rydberg atoms in the beam at the end of the decelerator, the field-ionization signal was monitored as a function of the delay time between photoexcitation and the application of the field-ionization pulse, all other parameters remaining constant. In the following, we shall refer to the data obtained from such measurements as time-of-flight (TOF) spectra. The velocity distribution of the helium atoms can be extracted from these TOF spectra using simple equations relating the total times of flight of the atoms to their position at excitation, the waveform switch-on time, the selected initial velocity, and the chosen acceleration, or using more sophisticated particle-trajectory-simulation methods. For the analysis of all results presented in this article, we have adapted the particle-trajectory-simulation program developed and used in our previous work on the Rydberg-Stark deceleration of atoms and molecules [17,30].

III. RESULTS

Figure 4 illustrates the use of the surface-electrode decelerator as a velocity selector. The figure displays time-of-flight spectra, each recorded using waveforms oscillating with a constant frequency ω and thus optimal to guide the subset of He Rydberg atoms in the beam moving with a longitudinal velocity around $v_z = 3d_z\omega/(2\pi)$. The experiments were carried out following excitation to $n = 30$, $k = 27$, and $m_\ell = 0$ Rydberg-Stark states. Compared to the TOF spectrum obtained without applying any waveform to the decelerator electrodes (solid black line in Fig. 4), which reflects the velocity distribution of the He Rydberg atoms in the supersonic beam, the TOF spectra obtained with these waveforms are characterized by a much narrower and more symmetric TOF distribution, with a full width at half maximum of about 2 μs. The velocities indicated above the maximal positions of these distributions
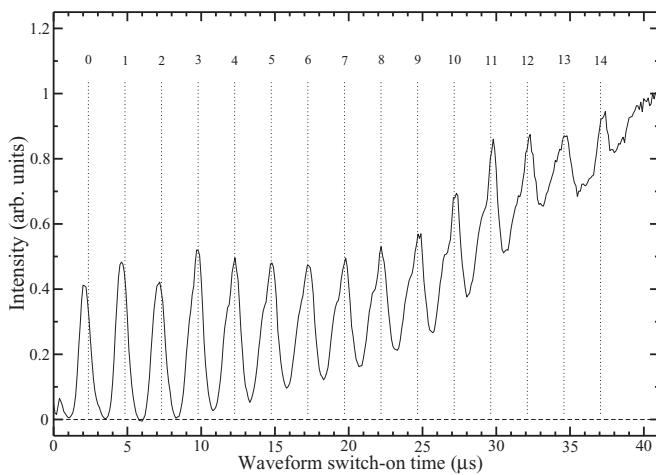
FIG. 3. Background-subtracted $n = 30$, $k = 27$, and $m_\ell = 0$ He Rydberg-atom signal as a function of the switch-on time of the waveforms used to guide atoms with an initial velocity of 1210 m/s above the surface-electrode decelerator. The maxima (labeled with integer numbers from 0 to 14) correspond to the times at which the atom cloud is centered at one of the 15 trap minima.
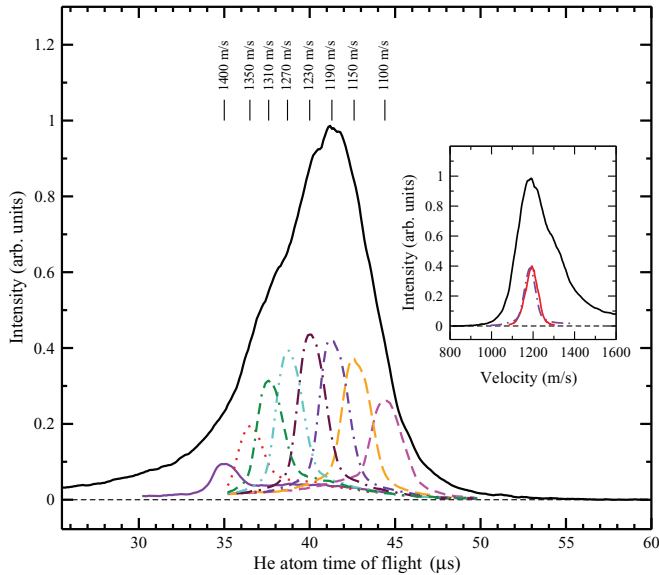
FIG. 4. (Color online) The $n = 30$, $k = 27$, and $m_\ell = 0$ He Rydberg-atom signal measured following pulsed-field ionization at the end of the decelerator as a function of the time between the laser-excitation pulse and the electric-field-ionization pulse. The solid black line was obtained without applying any waveforms to the decelerator electrodes. The colored traces were obtained using waveforms designed for selecting atoms moving with a selected initial velocity (given above the corresponding traces) and guiding these atoms at a constant velocity above the decelerator. The inset shows a comparison of the velocity distribution of atoms guided at 1190 m/s derived from particle-trajectory simulations (solid red line) and obtained from the time-of-flight distribution after conversion of the time-of-flight axis in a velocity axis (dash-dotted line).

are those one obtains from the oscillation frequencies of the waveforms used in these guiding experiments by means of Eq. (1). Converting the time-of-flight distributions into longitudinal velocity distributions leads to the conclusion that the velocity distribution of the beam has a half width of ≈ 100 m/s, corresponding to a longitudinal temperature of ≈ 2.4 K. The velocity distribution of the guided atoms at the end of the decelerator chip was determined by analyzing the results of particle-trajectory simulations and comparing calculated and experimental velocity distributions. The procedure is illustrated in the inset of Fig. 4, which compares the velocity distribution of atoms guided at 1190 m/s derived from the particle-trajectory simulation (solid red line) with that obtained experimentally (dash-dotted line). The two distributions are almost identical, which enables us to conclude that the half width at half maximum (≈ 30 m/s) of the distribution represents a good measure of the temperature (≈ 200 mK). The simulations also show that the initial velocity distributions of the particles loaded into the trap hardy broaden during the guiding process, indicating that heating effects are not significant. Narrower distributions can be obtained by initial selection of Rydberg-Stark states with a smaller value of k and thus a smaller electric dipole moment, however, at the expense of a reduced number of guided atoms. The relative strength of the pulsed-field-ionization signals indicates that about 12% of the initially excited Rydberg atoms can be loaded in a single moving trap and guided at a constant velocity over the PCB.

As explained in Sec. II, acceleration of the Rydberg atoms is achieved by accelerating the moving traps the atoms have been loaded into. To this end, the oscillation frequency of the waveforms is chosen to be time dependent, a constant acceleration being obtained with a linear frequency chirp. In the noninertial frame of reference with origin at the center of the moving trap, the effective potential energy of the atoms along the beam propagation axis can be described to a good approximation by [31,32]

$$U_{\text{eff}}(z') = U_0(z') + m a_z z', \qquad (2)$$

where $U_0(z')$ represents the potential resulting from the electric-field distribution, m is the mass of the atoms, a_z is the chosen acceleration, and z' is the position with respect to the potential minimum of the moving trap. In the case of deceleration (a_z negative), the effective potential is lowered in front of the trap minimum in the propagation direction, which reduces the phase-space acceptance of the trap and imposes a restriction on the maximal deceleration achievable.

In Fig. 5, the TOF distributions obtained for accelerations a_z ranging from -5.6×10^6 to -1.6×10^7 m/s^2 [Fig. 5(a)] are compared with the distributions extracted from particle-trajectory simulations [Fig. 5(b)]. These TOF spectra were measured by monitoring the He$^+$ ions produced by pulsed-field ionization in region (iv) of the decelerator (see Fig. 1) as a function of the delay between photoexcitation and the application of the electric-field pulse. The experiments were carried out following excitation to the $n = 30$, $k = 23$, and $m_\ell = 0$ Rydberg-Stark state. The top trace was obtained after guiding the Rydberg atoms at a constant velocity of 1200 m/s. The other traces were measured by applying linear frequency chirps to the decelerator electrodes to achieve accelerations between -5.6×10^6 and -1.6×10^7 m/s^2, as indicated above the respective traces. These accelerations were chosen so as to generate beams with final velocities of 1000, 800, 600, and 400 m/s, as given in Fig. 5(b). The traces in Fig. 5(a) consist of two peaks. The first one, centered at the time of flight of about 41 μs of the undecelerated beam, corresponds to atoms that are not decelerated and the second peak to the decelerated atoms. The TOF distributions obtained from particle-trajectory simulations presented in Fig. 5(b) are in good agreement with the experimental results, which enables us to estimate important characteristics of the decelerated beam directly from the simulations, such as its final velocity and its velocity distribution, which corresponds to a translational temperature of 55 mK in the case of a deceleration to a final velocity of 400 m/s. The width of the velocity distribution and the phase-space acceptance of the decelerator both increase with the electric dipole moment of the selected Stark states, as already noted in the discussion of Fig. 4, and decrease with increasing absolute value of the acceleration.

The dependence of the phase-space acceptance on the acceleration and the dipole moment is illustrated in more detail in Fig. 6, which compares the integrated TOF signals obtained for different Stark states ($k = 27$, 17, and 11) of the $n = 30$ and $m_\ell = 0$ manifold and for different accelerations in the range between -3.8×10^7 and -1.6×10^7 m/s^2. As expected, the largest phase-space acceptance is achieved for the Stark states having the largest dipole moments and for
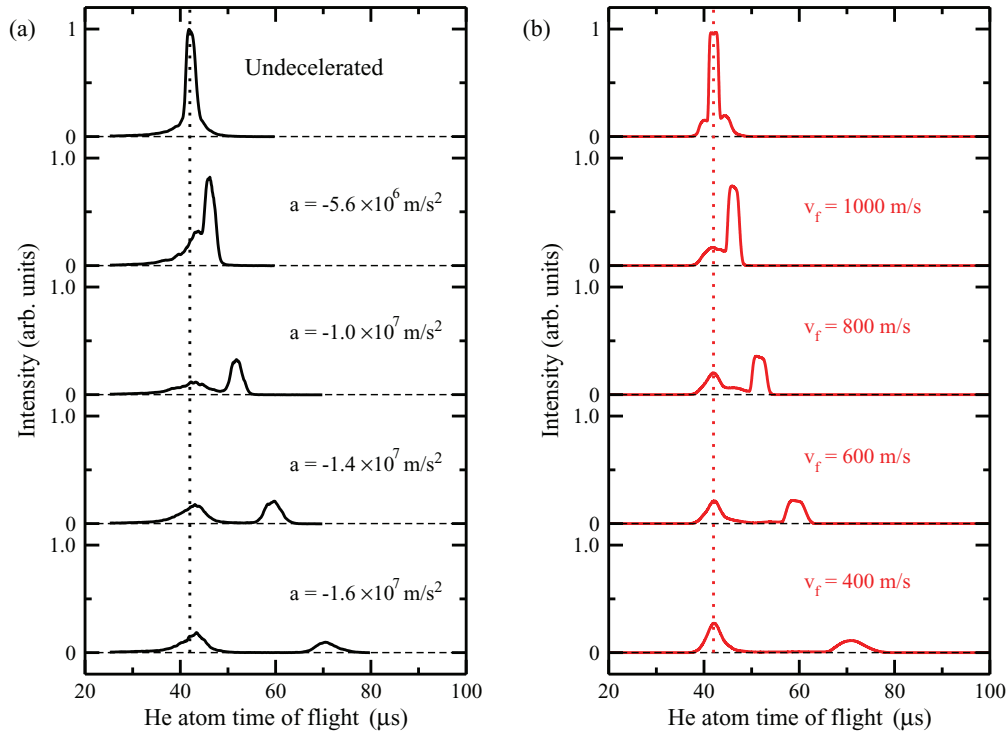
FIG. 5. (Color online) Deceleration of helium atoms prepared in the $n = 30$, $k = 23$, and $m_\ell = 0$ Rydberg-Stark state. The deceleration was achieved using waveforms designed for accelerations of -5.6×10^6, -1.0×10^7, -1.4×10^7, and -1.6×10^7 m/s^2 and final velocities of 1000, 800, 600, and 400 m/s, respectively, as indicated above the corresponding traces. The traces were obtained by monitoring the pulsed-field-ionization signal at the end of the decelerator as a function of the delay time between laser excitation and the application of the field-ionization pulse. (a) Experimental results. (b) Results of particle-trajectory simulations. The position corresponding to the undecelerated beam (velocity of 1200 m/s) is marked by a dashed vertical line.

the smallest absolute value of the acceleration. The observed behavior can be semiquantitatively described by a simple model based on Eq. (2) and on the size of the Rydberg-atom
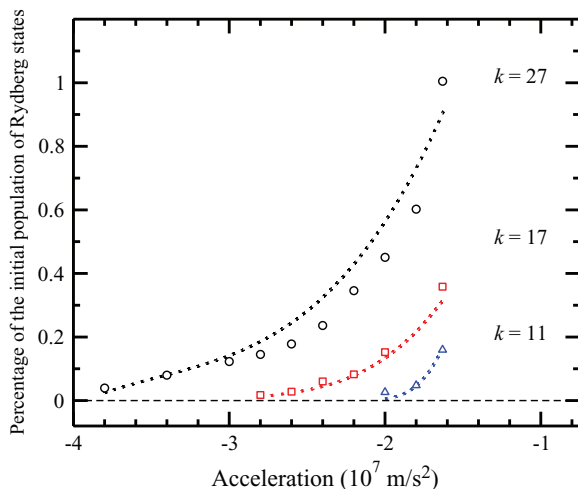
FIG. 6. (Color online) The $n = 30$ and $m_\ell = 0$ He Rydberg-atom signal measured by pulsed-field ionization at the end of the decelerator following deceleration using waveforms designed to achieve different accelerations, as given along the horizontal axis. The circles, squares, and triangles indicate measurements carried out for $k = 27$, 17, and 11 Rydberg-Stark states, respectively. The lines correspond to the results of calculations carried out to determine the phase-space acceptance of the decelerator.

cloud at the entrance of the decelerator. The diameter of this cloud is estimated to be about 1 mm from the laser spot size at excitation and considering the free propagation, with the longitudinal temperature of 2.4 K derived from Fig. 4, of the excited atoms over the 2.5 mm separating the photoexcitation point and the entrance of the decelerator. From the distributions of positions and velocities relative to the center of the traps, assumed to be Gaussian, one can directly determine the ratio of atoms having a total (potential and kinetic) energy larger than the saddle point of the potential given by Eq. (2). Assuming that the corresponding atoms are lost in the deceleration process leads to the dotted lines depicted in Fig. 6, which are in good agreement with the experimental data. This analysis indicates that, under our experimental conditions, at least 1% of the atoms initially prepared in the $n = 30$ and $k = 27$ Rydberg-Stark state can be decelerated as long as the absolute value of the acceleration does not exceed 1.7×10^7 m/s^2. This value reduces to $\approx 0.16\%$ for the $n = 30$ and $k = 11$ Rydberg-Stark state. In the experiments and the simulations presented in Fig. 6, we estimate that $\approx 10^5$ Rydberg atoms are generated in the photoexcitation volume so that the density of Rydberg atoms at the end of the deceleration is $\approx 4 \times 10^5$ cm^{-3} in the case of the $n = 30$ and $k = 27$ Rydberg-Stark state and $a = -1.7 \times 10^7$ m/s^2. These conclusions are supported by the results of numerical particle-trajectory simulations, which further indicate that a larger fraction of the initially prepared atoms could be decelerated by using a laser spot size of 100 μm diameter.
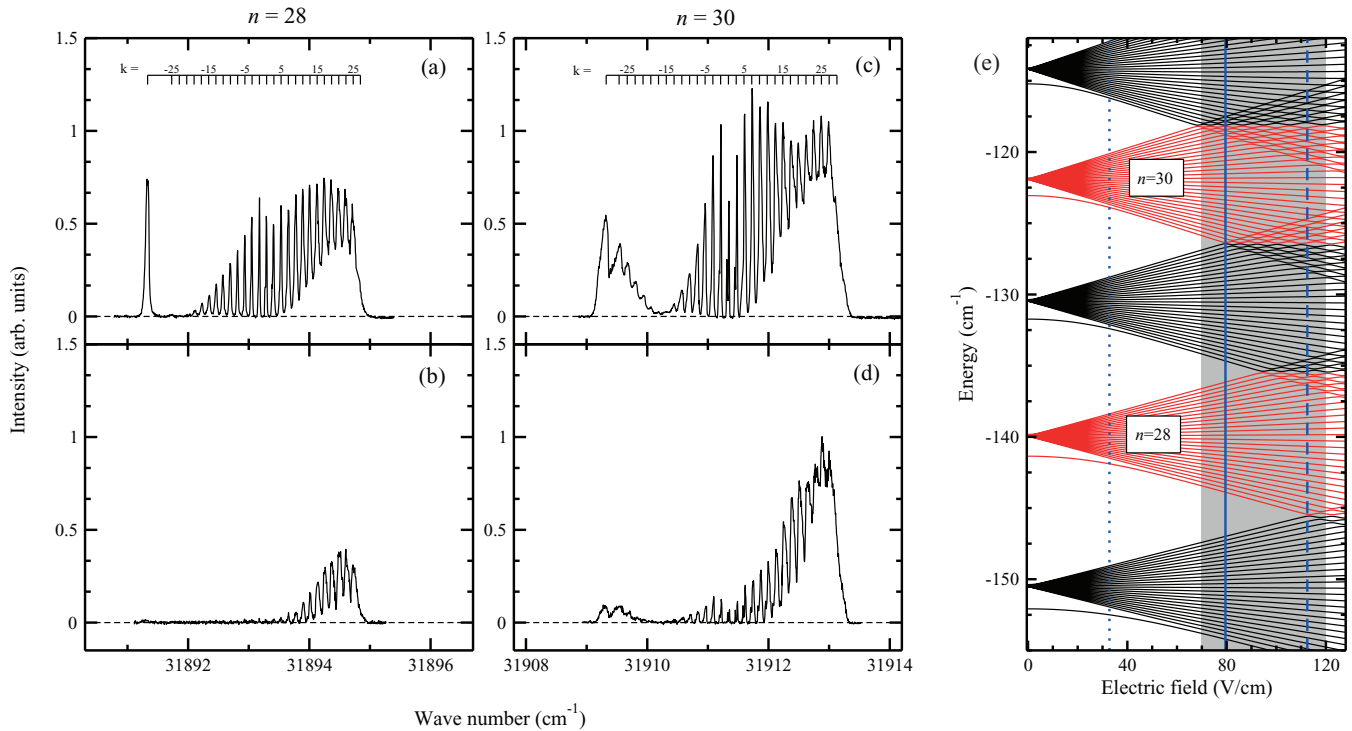
FIG. 7. (Color online) (a)–(d) Spectra of transitions to (a) and (b) $n = 28$ and (c) and (d) $n = 30$, $m_\ell = 0$ Rydberg-Stark states of He recorded following photoexcitation in the presence of an electric field of 32.8 V/cm and detection by pulsed-field ionization at the end of the decelerator. Traces (a) and (c) were recorded without applying any waveform to the decelerator electrodes. Traces (b) and (d) were obtained after deceleration from an initial velocity of 1200 m/s to a final velocity of 400 m/s. (e) Calculated Stark map of $m_\ell = 0$ Rydberg states of He. The shaded gray area corresponds to the range of electric-field strengths experienced by the atoms during the deceleration process. The dotted vertical line indicates the electric field at photoexcitation. The solid (dashed) vertical line represents the field at which the extreme Stark states of the $n = 29$ and 30 ($n = 27$ and 28) manifolds cross.

The spectra displayed in Figs. 7(a)–7(d) were recorded by monitoring the pulse-field-ionization signal at the end of the decelerator [region (iv); see Fig. 1] as a function of the laser excitation wave number in the vicinity of the $n = 28$ [Figs. 7(a) and 7(b)] and $n = 30$ [Figs. 7(c) and 7(d)] manifolds of Stark states. The electric field at excitation was 32.8 V/cm in all four cases. When comparing spectra obtained without applying any waveforms to the decelerator [Figs. 7(a) and 7(c)] with those obtained following deceleration to a final velocity of 400 m/s [Figs. 7(b) and 7(d)], one observes that the deceleration process selects atoms in Rydberg states with a positive k value, as expected. This effect is seen most clearly in the spectra recorded at $n = 28$, which show that only atoms in $k \geqslant 11$ Rydberg-Stark states, with dipole moments of more than about $450\,a_0 e$, are efficiently decelerated. The situation is different at $n = 30$, where one observes signals corresponding to atoms initially prepared in Stark states with k values below -25. These atoms have dipole moments oriented in the wrong direction and should have been rejected by the decelerator. The Stark map depicted in Fig. 7(e) provides a qualitative explanation for this unexpected behavior: At the time of photoexcitation, the electric field is ≈ 33 V/cm at the position where the laser beam intersects the atom beam. This field, indicated by a vertical dotted line, is located well below the field, known as the Inglis-Teller field [33], at which the Stark manifolds of neighboring n values start overlapping. The Inglis-Teller fields corresponding to the

$n = 28$ and 30 manifolds are marked by dashed and solid vertical lines, respectively. The maximal values of the electric fields the atoms are subject to during the switch-on process of the waveforms correspond to the range indicated by the shaded area in Fig. 7(e). This range of fields is beyond the Inglis-Teller field for $n = 30$, but below this field for $n = 28$, so the atoms in the $n = 28$ Rydberg-Stark state do not undergo dipole-inverting transitions. During the initial trap-loading process, the atoms experience varying electric fields and those initially prepared in $n = 30$ Rydberg states and located close to the edge of the trap, where the electric field is largest, can make a transition from an $n = 30$ and $k < 0$ Stark state to an $n = 29$ and $k > 0$ one by adiabatic traversal of an avoided crossing and therefore be subsequently decelerated. For these atoms to be decelerated to the desired velocity, however, it is necessary for the transition to take place in the initial phase of the deceleration process.

Figure 8 summarizes the results of a series of experiments in which helium atoms initially excited to the $n = 30$, $k = 23$, and $m_\ell = 0$ Stark state were decelerated to zero velocity, held in the stationary traps for a trapping time adjustable between 0 and 50 μs, and then reaccelerated to a final velocity of 400 m/s before being detected in region (iv) of the decelerator. Whereas the origin of the bottom TOF axis was chosen to coincide with the photoexcitation laser pulse, the origin of the upper TOF axis was placed at the maximum of the TOF distribution corresponding to the measurement
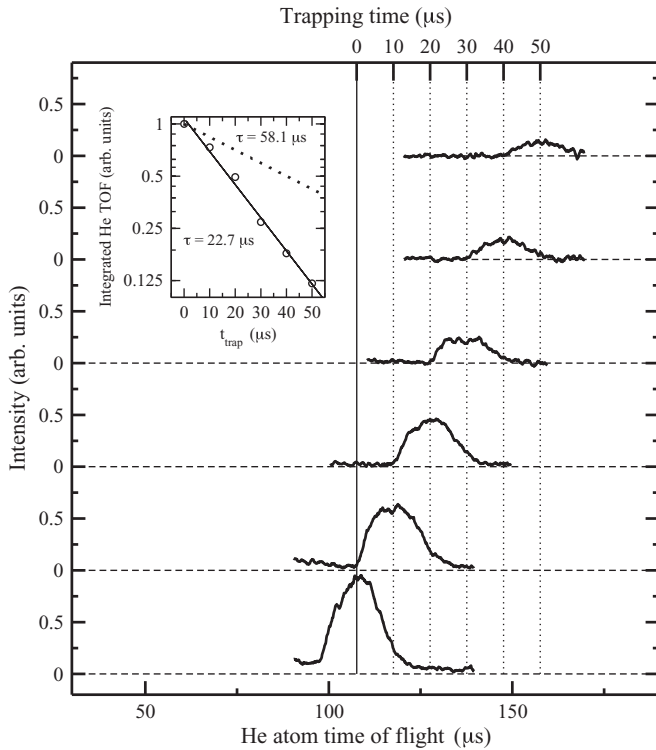
FIG. 8. Rydberg-atom signal obtained at the end of the decelerator following deceleration, trapping, and reacceleration of helium atoms prepared in the $n = 30$, $k = 23$, and $m_\ell = 0$ Rydberg states. The inset shows the integrated signal as a function of the time the trap remained stationary on the chip (solid line) and the expected radiative decay (dotted line).

made for 0 trapping time (solid vertical line in Fig. 8). In this way, one immediately sees that the maxima of the other TOF distributions, marked by dotted vertical lines, are exactly shifted by the trapping times the waveforms were programmed for. The integrated intensity of the TOF spectra is depicted as a function of the trapping time in the inset of Fig. 8. It decays exponentially with a time constant of ≈ 25 μs, which is shorter than the expected fluorescence time of the $n = 30$, $k = 23$, and $m_\ell = 0$ Stark states (≈ 58 μs according to our calculations). We attribute the lifetime reduction to

collisions with ground-state He atoms in the trailing part of the 200-μs-long gas pulses with a weaker but non-negligible contribution of ionization induced by blackbody radiation and possibly also of processes resulting from the proximity of the surface of the decelerator.

IV. CONCLUSION

The experiments presented in this article demonstrate that it is possible to decelerate fast supersonic beams using a surface-electrode Rydberg-Stark decelerator. With such a device, the final velocity of the beams can be tuned in a straightforward manner by solely changing the waveforms applied to the electrodes. Moreover, the width of the velocity distribution can be adjusted by selecting Rydberg-Stark states of different electric dipole moments, however with consequences on the total number of decelerated atoms. The ability to control both the velocity and the velocity spread of the atomic beams makes the decelerator attractive for studies of collisions between Rydberg atoms and atoms, molecules, and surfaces.

The results presented in Fig. 8 further show that surface-electrode decelerators can be used to trap Rydberg atoms above a surface. This aspect is expected to represent an asset for experiments aimed at studying the interaction of Rydberg atoms with surfaces [34] and at coherently manipulating the quantum states of Rydberg states using fields emanating from on-chip microwave transmission lines [21] and superconducting microwave cavities [35].

The initial kinetic energy of a helium atom (4 nucleons) moving at 1200 m/s corresponds to the initial kinetic energy of an atom of 40 nucleons entrained in a supersonic expansion of Xe with a typical velocity of 350 m/s. We therefore expect that a wide range of atoms and molecules could be trapped with the decelerator described in this article.

[1] H. L. Bethlem, G. Berden, and G. Meijer, Phys. Rev. Lett. **83**, 1558 (1999).

[2] S. D. Hogan, M. Motsch, and F. Merkt, Phys. Chem. Chem. Phys. **13**, 18705 (2011).

[3] S. Y. van de Meerakker, H. L. Bethlem, N. Vanhaecke, and G. Meijer, Chem. Rev. **112**, 4828 (2012).

[4] E. Narevicius and M. G. Raizen, Chem. Rev. **112**, 4879 (2012).

[5] J. van Veldhoven, J. Küpper, H. L. Bethlem, B. Sartakov, A. J. A. Roij, and G. Meijer, Eur. Phys. J. D **31**, 337 (2004).

[6] L. Scharfenberg, S. Y. T. van de Meerakker, and G. Meijer, Phys. Chem. Chem. Phys. **13**, 8448 (2011).

[7] J. J. Gilijamse, S. Hoekstra, S. A. Meek, M. Metsälä, S. Y. T. van de Meerakker, G. Meijer, and G. C. Groenenboom, J. Chem. Phys. **127**, 221102 (2007).

[8] Ch. Seiler, S. D. Hogan, H. Schmutz, J. A. Agner, and F. Merkt, Phys. Rev. Lett. **106**, 073003 (2011).

[9] B. Stuhl, M. Hummon, M. Yeo, G. Quemener, J. Bohn, and J. Ye, Nature (London) **492**, 396 (2012).

[10] R. Fulton, A. I. Bishop, and P. F. Barker, Phys. Rev. Lett. **93**, 243004 (2004).

[11] S. Merz, N. Vanhaecke, W. Jäger, M. Schnell, and G. Meijer, Phys. Rev. A **85**, 063411 (2012).

[12] S. R. Procter, Y. Yamakita, F. Merkt, and T. P. Softley, Chem. Phys. Lett. **374**, 667 (2003).

[13] S. D. Hogan, Ch. Seiler, and F. Merkt, Phys. Rev. Lett. **103**, 123001 (2009).

[14] A. Osterwalder, S. A. Meek, G. Hammer, H. Haak, and G. Meijer, Phys. Rev. A **81**, 051401 (2010).

[15] A. Trimeche, M. Bera, J.-P. Cromires, J. Robert, and N. Vanhaecke, Eur. Phys. J. D **65**, 263 (2011).

[16] E. Lavert-Ofir, S. Gersten, A. B. Henson, I. Shani, L. David, J. Narevicius, and E. Narevicius, New J. Phys. **13**, 103030 (2011).

[17] S. D. Hogan, P. Allmendinger, H. Sassmannshausen, H. Schmutz, and F. Merkt, Phys. Rev. Lett. **108**, 063008 (2012).

[18] S. A. Meek, H. Conrad, and G. Meijer, Science **324**, 1699 (2009).

[19] G. R. Lloyd, S. R. Procter, E. A. McCormack, and T. P. Softley, J. Chem. Phys. **126**, 184702 (2007).

[20] E. So, M. Dethlefsen, M. Ford, and T. P. Softley, Phys. Rev. Lett. **107**, 093201 (2011).

[21] S. D. Hogan, J. A. Agner, F. Merkt, T. Thiele, S. Filipp, and A. Wallraff, Phys. Rev. Lett. **108**, 063004 (2012).

[22] S. A. Meek, G. Santambrogio, H. Conrad, and G. Meijer, J. Phys. Conf. Ser. **194**, 012063 (2009).

[23] A. Emmert, A. Lupacu, G. Nogues, M. Brune, J.-M. Raimond, and S. Haroche, Eur. Phys. J. D **51**, 173 (2009).

[24] J. D. Carter, O. Cherry, and J. D. D. Martin, Phys. Rev. A **86**, 053401 (2012).

[25] A. Tauschinsky, R. M. T. Thijssen, S. Whitlock, H. B. van Linden van den Heuvell, and R. J. C. Spreeuw, Phys. Rev. A **81**, 063411 (2010).

[26] H. Hattermann, M. Mack, F. Karlewski, F. Jessen, D. Cano, and J. Fortágh, Phys. Rev. A **86**, 022511 (2012).

[27] M. Raunhardt, M. Schäfer, N. Vanhaecke, and F. Merkt, J. Chem. Phys. **128**, 164310 (2008).

[28] T. Halfmann, J. Koensgen, and K. Bergmann, Meas. Sci. Technol. **11**, 1510 (2000).

[29] S. A. Meek, H. L. Bethlem, H. Conrad, and G. Meijer, Phys. Rev. Lett. **100**, 153003 (2008).

[30] E. Vliegen, P. Limacher, and F. Merkt, Eur. Phys. J. D **40**, 73 (2006).

[31] S. A. Meek, H. Conrad, and G. Meijer, New J. Phys. **11**, 055024 (2009).

[32] S. D. Hogan, Ch. Seiler, and F. Merkt, J. Phys. B **46**, 045303 (2013).

[33] T. F. Gallagher, *Rydberg Atoms* (Cambridge University Press, Cambridge, 1994).

[34] E. A. McCormack, E. So, M. Dethlefsen, M. S. Ford, and T. P. Softley, J. Phys. B **45**, 015204 (2012).

[35] A. Wallraff, D. Schuster, A. Blais, L. Frunzio, Huang, J. Majer, S. Kumar, S. Girvin, and R. Schoelkopf, Nature (London) **431**, 162 (2004).